Publ. Astron. Soc. Japan (2018) 70 (3), 33 (1–8)
doi: 10.1093/pasj/psy021
Advance Access Publication Date: 2018 March 22

Correlation between SiO $v = 3$ $J = 1 \rightarrow 0$ maser excitation and the light curve of a long-period variable star

Miyako Oyadomari,[1,*] Hiroshi Imai,[1] Takumi Nagayama,[2] Tomoaki Oyama,[2] Naoko Matsumoto,[2] Jun-ichi Nakashima,[3] and Se-Hyung Cho[4]

[1]Graduate School of Science and Engineering, Kagoshima University, 1-21-35 Korimoto, Kagoshima, Kagoshima 890-0065, Japan
[2]Mizusawa VLBI Observatory, National Astronomical Observatory of Japan, 2-12 Hoshigaoka, Mizusawa, Oshu, Iwate 023-0861, Japan
[3]Department of Astronomy and Geodesy, Ural Federal University, Lenin Ave. 51, Ekaterinburg 620000, Russia
[4]Korea Astronomy and Space Science Institute, 776 Daedeokdae-ro, Yuseong-gu, Daejeon 305-348, Korea

*E-mail: k7219031@kadai.jp

Received 2017 November 6; Accepted 2018 February 7

Abstract

In order to understand the excitation mechanisms of silicon monoxide (SiO) masers around long-period variables (LPVs), we have investigated distributions of the SiO $v = 2$ and $v = 3$ $J = 1 \rightarrow 0$ masers around 12 LPVs by very long baseline interferometry (VLBI) observations with the VLBI Exploration of Radio Astrometry (VERA) and the Nobeyama 45 m telescopes. VLBI fringes of the $v = 3$ maser emission were detected for five LPVs. The composite maps of the $v = 2$ and $v = 3$ masers were made for T Cep, W Hya, WX Psc, and R Leo using the spectral line phase-referencing technique. The $v = 2$ maser spots were distributed in a ring-like form around the central stars, while it is difficult to recognize any specific morphology in the $v = 3$ maser distributions due to the small number of $v = 3$ spots detected. However in T Cep, we find that the distribution of the $v = 3$ maser spots correlates well with the $v = 2$ masers within a few milliarcseconds (0.2–0.3 au) in position and 1 km s^{-1} in line-of-sight velocity at the light curve phase of $\phi = 0.28$ ($\phi = 0.0$ and 1.0 correspond to the visible light maxima). This correlation implies that the mechanism of line-overlapping between the mid-infrared lines of H_2O and SiO molecules works in T Cep at $\phi = 0.28$. We discuss the possibility that the line-overlapping may work at the limited duration from the maximum to the minimum of the stellar light curve.

Key words: masers — stars: AGB and post-AGB

1 Introduction

Very long baseline interferometry (VLBI) observations are an excellent way to investigate the kinematics of the gas released from the surface of long-period variable (LPV) stars. This is particularly the case when we observe silicon monoxide (SiO) maser emission seen within 1–2 stellar radii of the stellar surface as a probe to investigate the gas clump motion and the temporal variation of the physical environments of the innermost parts of circumstellar envelopes

(CSEs). Gonidakis, Diamond, and Kemball (2013) present a movie of SiO $v = 1$ $J = 1 \rightarrow 0$ masers toward a Mira variable TX Cam, in which they show that the ring of the $v = 1$ masers seems to be moving together with a shock created in every pulsation cycle and propagating outward at a velocity of $\sim$7 km s^{-1}. Since the maser emission of the $J = 1 \rightarrow 0$ $v = 1$ line is detected in a slow stellar wind, one may think that the maser pumping by shock occurs throughout the whole pulsation cycle. However, the behaviors of other maser lines, such as the $J = 1 \rightarrow 0$ lines at higher vibrational levels, e.g., $v = 2$ and $v = 3$, should also be consistently understood with the $v = 1$ maser in terms of the correlation with shock waves and/or other factors such as stellar radiation.

There are three major conceivable models explaining the excitation of circumstellar SiO masers: pumping by (1) stellar radiation; (2) collisions with hydrogen molecules (collisional pumping); and (3) mid-infrared (MIR) radiation from H_2O molecules in CSEs (line-overlapping; e.g., Olofsson et al. 1981; Lockett & Elitzur 1992; Bujarrabal 1994; Desmurs el al. 2014). The results of previous VLBI observations suggest that the dominant excitation mechanism depends on the type of the star. Soria-Ruiz et al. (2004) performed VLBI observations towards the oxygen-rich star WX Psc and the S-type star χ Cyg. In these observations, the $v = 2$ $J = 1 \rightarrow 0$ maser line was detected in both sources, while the $v = 2$ $J = 2 \rightarrow 1$ maser line was detected only in χ Cyg. Interestingly, in the case of WX Psc, the distributions of the $J = 1 \rightarrow 0$ $v = 1$ and $v = 2$ lines are quite similar to each other, while the region of the $J = 2 \rightarrow 1$ $v = 1$ line is 1.5 times as distant from the central star compared to those of the $J = 1 \rightarrow 0$ lines. The absence of the $v = 2$ $J = 2 \rightarrow 1$ masers and the maser distributions in WX Psc mentioned above were explained by the following scheme of line-overlapping between the H_2O and SiO transitions. In this scheme, the MIR transition of H_2O $11_{6,6}$ $\nu_2 = 1 \rightarrow 12_{7,5}$ $\nu_2 = 0$ ($\Delta\lambda$= 8.2025 μm) excites SiO molecules from $v = 1$ $J = 0$ to $v = 2$ $J = 1$ ($\Delta\lambda$ = 8.2024 μm; Olofsson et al. 1981). The separation is only 1.0 km s^{-1} between the line-of-sight velocities corresponding to the Doppler-shifted wavelengths of the two MIR lines. With this pumping by the H_2O MIR line, the population inversion between the $v = 2$ $J = 0$ and $v = 2$ $J = 1$ levels are enhanced, while that between the $v = 2$ $J = 1$ and $v = 2$ $J = 2$ levels is quenched. The difference of the emission regions between the $v = 1$ $J = 2 \rightarrow 1$ and $v = 1$ $J = 1 \rightarrow 0$ lines observed in WX Psc could be naturally interpreted by the line-overlapping (Soria-Ruiz et al. 2004). Cho, Lee, and Park (2007) conducted single-dish observations towards an oxygen-rich star TX Cam and S-type star χ Cyg and found that the $v = 3$ $J = 2 \rightarrow 1$ maser line was detected in χ Cyg but not in TX Cam, although the $v = 3$ $J = 3 \rightarrow 2$ maser line was detected. They suggested that the absence of the $v = 3$ $J = 2 \rightarrow 1$ maser in TX Cam is caused by line-overlapping between the H_2O $5_{0,5}$ $\nu_2 = 2 \rightarrow 6_{3,4}$ $\nu_2 = 1$ ($\Delta\lambda = 8.23312$ μm) and SiO $v = 2$ $J = 0$ to $v = 3$ $J = 1$ lines, of which the corresponding velocity difference is 1.5 km s^{-1}. Since the emission regions of the two H_2O MIR lines, which are overlapped with SiO MIR lines, could coexist, one could expect that the SiO maser lines of $v = 1$, $v = 2$, and $v = 3$ $J = 1 \rightarrow 0$ show a correlation with each other in the spatial and velocity distributions of their emission regions.

Imai et al. (2010) found that the $v = 2$ and $v = 3$ $J = 1 \rightarrow 0$ SiO maser lines behaved in different ways in the time variation of the emission regions through their VLBI observations for the oxygen-rich star W Hya at the light curve phases of $\phi = 0.11$ and $\phi = 0.22$. The emission regions of the $v = 2$ and $v = 3$ lines coexist only at the second epoch. Their result implies that the line-overlapping in the $v = 2$ $J = 0$ to $v = 3$ $J = 1$ transition works in the limited duration of the light curve cycle. A possible explanation is that the line-overlapping occurs only when infrared radiation from the star (and the external dust region) is strong enough to excite H_2O molecules in CSEs. This could be confirmed with a simultaneous VLBI monitoring of the $v = 2$ and $v = 3$ $J = 1 \rightarrow 0$ maser lines towards a set of LPVs that share similar observational properties. Here we report the results of VLBI observations of the $v = 2$ and $v = 3$ $J = 1 \rightarrow 0$ lines towards 12 LPVs, with the aim of exploring the possible correlation between the maser excitation and light curve phase.

Note that we use the HITRAN (High resolution TRANsmission molecular absorption database) 2016 edition to obtain the wavenumbers of the spectral line transition (Gordon et al. 2017). Note also that the wavelength of the SiO line transition ($\Delta\lambda = 8.221780$ μm) described in Gray (2012) was derived by using the molecular parameters for SiO from Tipping and Chackerian (1981). However, the difference of the wavelength from that of the H_2O line transition corresponds to a velocity of $\sim$730 km s^{-1}. Here we adopt the wavelength value of Olofsson et al. (1981).

2 Observations and data reduction

We carried out the VLBI observations of SiO $v = 2$ and $v = 3$ $J = 1 \rightarrow 0$ masers toward 12 LPVs (WX Psc, U Ori, AP Lyn, VY CMa, R Leo, W Hya, RS Vir, RU Her, U Her, V4120 Sgr, V1111 Oph, and T Cep, selected from Cho et al. 1996) using the four 20 m telescopes of VLBI Exploration of Radio Astrometry (VERA) and the 45 m telescope of Nobeyama Radio Observatory (NRO) on 2012 March 24–25 and May 21–22. In the first epoch, it was only possible to synthesize the maser images from the data obtained

Table 1. Parameters of the observed stars.

Source name	RA (J2000.0)	Dec (J2000.0)	Dist. [pc]	Ref.*	Epoch†	Phase‡	Scan§ [hr]	S / (1 σ noise)‖ [Jy] $v=2$	S / (1 σ noise)‖ [Jy] $v=3$	Synthesized beam#
WX Psc	$01^h06^m25^s.99$	$+12°35'53''.4$	1300	a	A	N/A	0.5	N / (0.15)	N / (0.15)	
					B	N/A	2.6	79 / (0.07)	1.8^+ / (0.17)	0.99 × 0.73, −65.4
U Ori	$05^h55^m49^s.17$	$+20°10'30''.7$	280	a	A	0.02	0.9	1.3 / (0.20)	N / (0.22)	
AP Lyn	$06^h34^m34^s.88$	$+60°56'33''.2$	N/A		B	N/A	1.3	5.4 (0.09)	N / (0.08)	
VY CMa	$07^h22^m58^s.32$	$-25°46'03''.0$	1150	b	A	0.87	2.3	109 / (0.07)	N / (0.08)	
R Leo	$09^h47^m33^s.48$	$+11°25'14''.2$	100	c	A	0.00	3.1	28 / (0.03)	3.4^- / (0.05)	
					B	0.18	3.8	216 / (0.05)	6.8^+ / (0.13)	1.42 × 0.84, −36.4
W Hya	$13^h49^m01^s.93$	$-28°22'04''.6$	90	c	A	0.88	2.3	36 / (0.08)	1.3^- / (0.12)	
					B	0.03	2.8	320 / (0.16)	63^+ / (0.09)	1.85 × 0.55, −25.1
RS Vir	$14^h27^m16^s.39$	$+4°40'41''.1$	610	c	B	0.15	0.9	1.5 / (0.10)	N / (0.08)	
RU Her	$16^h10^m14^s.52$	$+12°04'14''.3$	530	a	A	0.77	1.5	N / (0.06)	N / (0.06)	
U Her	$16^h25^m47^s.47$	$+18°53'32''.9$	360	a	A	0.19	1.6	45 / (0.08)	N / (0.07)	
V4120 Sgr	$18^h03^m56^s.53$	$-20°19'00''.5$	N/A		B	N/A	2.8	40 / (0.12)	2.6^- / (0.06)	
V1111 Oph	$18^h37^m19^s.26$	$+10°25'42''.2$	650	a	A	N/A	2.3	11 / (0.08)	N / (0.06)	
T Cep	$21^h09^m31^s.78$	$+68°29'27''.2$	170	c	A	0.14	2.6	5.8 / (0.06)	0.7^- / (0.05)	
					B	0.28	2.6	97 / (0.05)	3.0^+ / (0.05)	1.22 × 0.56, −52.3

*References: (a) Chibueze et al. (2016); (b) Choi et al. (2008); (c) Whitelock, Fest, and van Leeuwen (2008).
†Observation epoch in 2012. A: March 24 – 25, B: May 21 –22.
‡Light curve phase when the star was observed (0.0 and 1.0 at the light maximum). The light curve profiles of WX Psc, AP Lyn, V4120 Sgr, and V1111 Oph were too ambiguous to estimate the phases.
§Total integration time in hours.
‖The peak cross-power flux densities of the $v=2$ and $v=3$ $J=1\rightarrow 0$ masers and 1 σ noise levels yielded with the baseline between NRO and VERA Mizusawa. $^+$: The maser fringe of the $v=3$ line was detected and the composite map of the $v=2$ and $v=3$ masers was obtained successfully. $^-$: The maser fringe of the $v=3$ line was detected but it was too faint to be detected above a 5 σ noise level on the map. N: No detection of maser fringes above a 3 σ noise level.
#Major and minor axis lengths (mas) and position angle (°) of the elliptial synthesized beam.

from three telescopes of VERA and NRO because of insufficient observation time. Table 1 details the parameters of the observed stars and the observations. To investigate the relation between the maser distributions of the two lines and the optical light curve, the phases of the light curve were derived by using the photometric data provided by the American Association of Variable Star Observers (AAVSO) and given in table 1.

A target maser and position reference sources were observed simultaneously with the VERA telescopes using their dual beam receiving system, enabling high accuracy astrometry for the maser source. On the other hand, the NRO telescope observed only the maser sources but with higher sensitivity. The combination of the VERA and NRO telescopes covers baseline lengths from 400 km to 2300 km, consequently enabling us to detect maser emission fainter and more extended than those observed with VERA only. These telescopes commonly observed bright continuum sources for 3 min every 40 min for calibration of instrumental group delays, clock drifts, and bandpass characteristics. VERA was equipped with two types of tape recording systems, Sony DIR 1000 and DIR 2000, with signal recording rates of 128 Mbps and 1024 Mbps, respectively, yielding two and 16 baseband channels (BBCs) each with a bandwidth of 16 MHz. These systems were used simultaneously in the VERA stations, while only the former was used in NRO, where the two BBCs were assigned to the frequencies of the $v=2$ and $v=3$ maser lines. In data correlation by a Mitaka FX correlator, each of the maser BBCs was split into 512 spectral channels, corresponding to a velocity channel spacing of 0.22 km s^{-1} for the $v=2$ masers. The results of astrometry in the same observations but using only the data from VERA were published separately by Imai et al. (2012). Note that the astrometry with VERA was successful only for WX Psc and W Hya.

For data analysis, we used the Astronomical Image Processing System (AIPS) and the ParselTongue package, whose Python library enables us to handle the AIPS tasks externally using Python scripts. The spectral line phase-referencing technique was used for the composition of the $v=2$ and $v=3$ maser maps. This technique was used to synthesize composite maser maps in Imai et al. (2010, 2012) and Oyama et al. (2016). In this technique, we selected the visibility data in the velocity channel including the brightest but still simple-structured component of the $v=2$ maser for fringe fitting and self-calibration, whose solutions were applied to the data of the remaining $v=2$ and $v=3$ masers to synthesize the final image cubes. The $v=3$ maser map

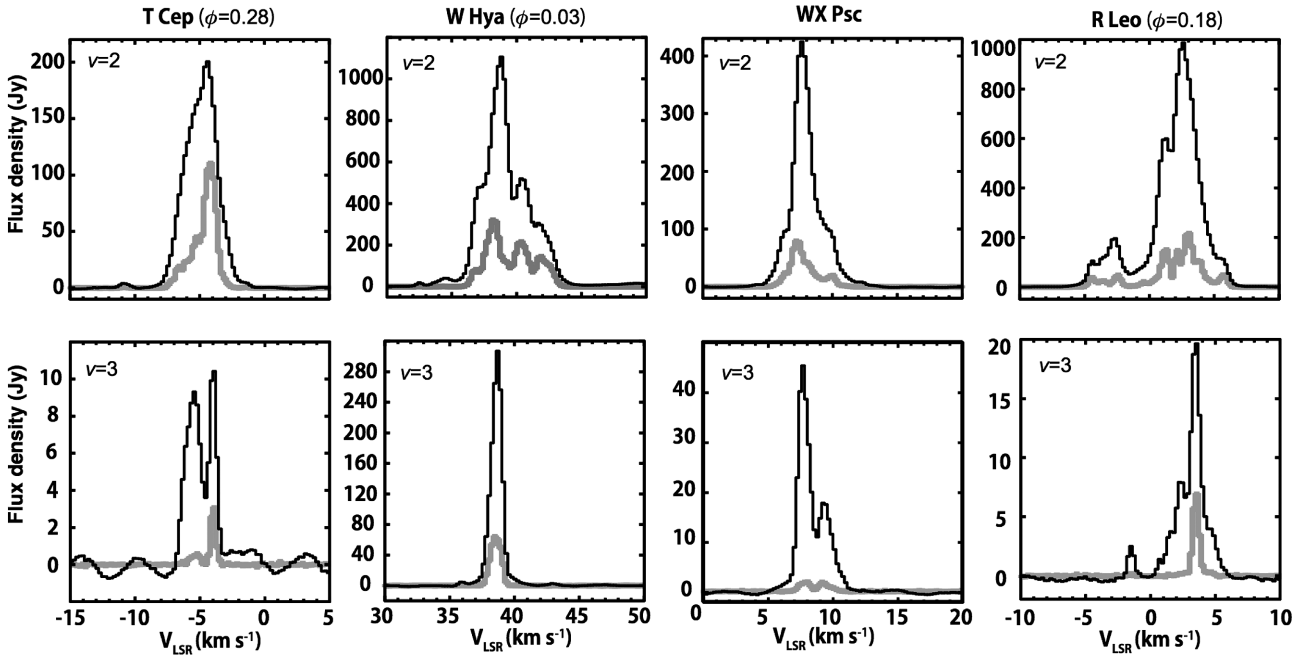

Fig. 1. Total-power spectra (black line) obtained by NRO and cross-power spectra (gray line) obtained from the baseline between NRO and Mizusawa stations of SiO $v = 2$ and $v = 3$ ($J = 1 \rightarrow 0$) masers towards T Cep, W Hya, WX Psc, and R Leo, which were observed on 2012 May 21–22.

was registered with respect to the position of the reference $v = 2$ maser spot. The positions of the $v = 3$ masers, however, would cause systematic shifts, which were attributed to the offset of the phase-tracking center from the true position of the reference maser spot. Such a shift is proportional to this offset and the difference in the frequencies between the $v = 2$ and $v = 3$ masers, about 304 MHz. To calculate the shift, the true maser position was determined by astrometry towards WX Psc and W Hya (Imai et al. 2012). Through this position correction, the uncertainty of the map registration was reduced to $\sim$50 μas. In other sources, we roughly calculated the absolute maser positions from the positions of the central stars and their proper motions cited from the SIMBAD Astronomical Database (cf. van Leeuwen 2007). The phase-referencing technique would also be significantly affected for the data including the NRO telescope by the station position error of the antenna, which was estimated to be a few tens of centimeters (Oyama et al. 2016). It would cause relative position errors of the $v = 2$ and $v = 3$ maser spots within a few mas in the composition maps.

3 Results

The $v = 3$ maser fringes were detected towards WX Psc, R Leo, W Hya, V4120 Sgr, and T Cep. However, in the case of R Leo, W Hya, and T Cep observed in the first epoch and V4120 Sgr observed in the second epoch, the $v = 3$ maser fringes were too faint to be detected above a 5 σ noise level on the maps. The peak cross-power flux densities of the SiO $v = 2$ and $v = 3$ $J = 1 \rightarrow 0$ masers are listed in table 1. Figure 1 shows the total-power spectra taken with NRO, and the cross-power spectra taken with the baseline between NRO and VERA Mizusawa of the $v = 2$ and $v = 3$ $J = 1 \rightarrow 0$ for the four LPVs for which the composite maps of the two maser lines were obtained successfully. The baselines of the spectra, especially of the $v = 3$ masers in which their profiles are zoomed more highly, are affected by instrumental standing waves even after subtracting the bandpass characteristics. The peak total-power flux densities of the $v = 3$ masers are 2%–27% of those of the $v = 2$ masers. The peak cross-power flux densities are 4%–55% of the total-power ones in both the $v = 2$ and $v = 3$ masers. The reduction in the cross-power flux densities compared to the total-power ones indicates that these masers have sizes comparable to a typical apparent size of a group of SiO maser spots, $\sim$0.1–4 au corresponding to $\sim$1–5 mas for our target sources (e.g., Soria-Ruiz et al. 2004; Imai et al. 2010; Gonidakis et al. 2013; Desmurs el al. 2014; Yun et al. 2016), resulting in detections of only compact parts of maser spots by the synthesized beams of the present VLBI observations ($\sim$1 mas). Therefore, we consider that the $v = 2$ and $v = 3$ maser gas clumps coexist within the spot size scale if the compact maser spots detected in the present VLBI observations are apparently coincident within this scale.

Figures 2, 3, 4, and 5 show the composite maps of the $v = 2$ and $v = 3$ masers towards T Cep, W Hya, WX Psc, and R Leo, respectively. The distributions of the $v = 2$ masers

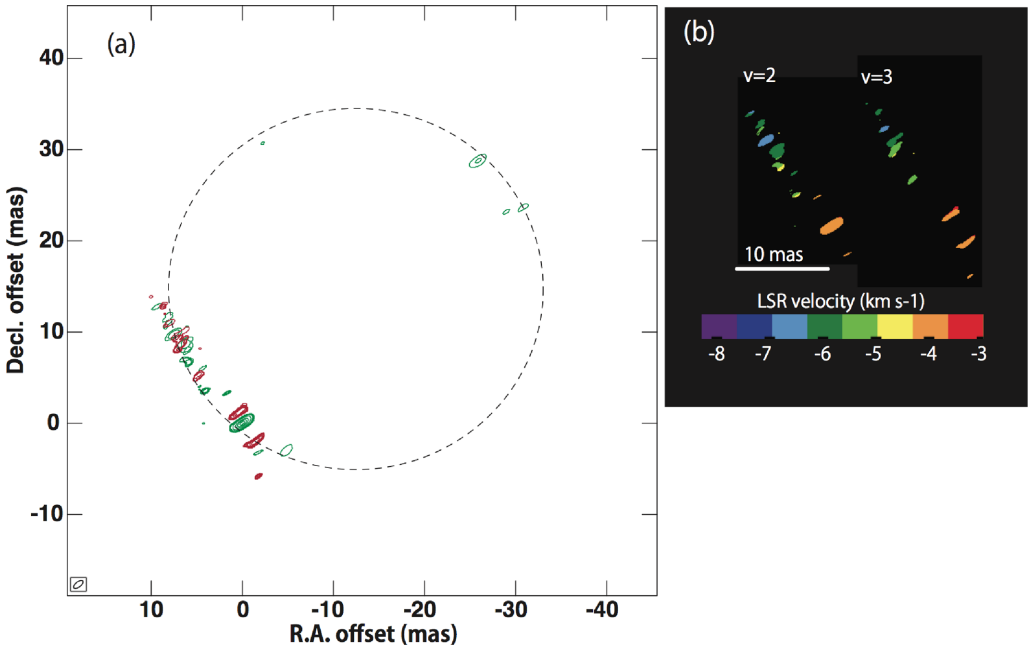

Fig. 2. Composite map of SiO masers of $v = 2$ (green) and $v = 3$ (red) ($J = 1 \rightarrow 0$) around T Cep observed on 2012 May 22 ($\phi = 0.28$). (a) Velocity-integrated contour map of the $v = 2$ and $v = 3$ masers. The systematic position shifts of the $v = 3$ masers from the reference $v = 2$ maser spot was corrected. The dashed circle is drawn so as to fit to the $v = 2$ maser distribution with a diameter of 40 mas to examine the possible existence of a ring morphology. The brightest maser spots of the $v = 2$ and the $v = 3$ masers are located at (0 mas, 0 mas) and (1 mas, 1 mas), respectively. The contour levels are set at 0.8, 4, 8, 20, 40, 56, and 72 Jy km s^{-1} beam^{-1} for the $v = 2$ masers and 0.02, 0.12, 0.24, 0.6, 1.2, 1.7, and 2.1 Jy km s^{-1} beam^{-1} for the $v = 3$ masers. The ellipse at the bottom-left corner shows the synthesized beam pattern. (b) First moment maps of the $v = 2$ and $v = 3$ masers. The $v = 3$ masers are shifted by 13 mas to the west side from the position of those in the composite map.

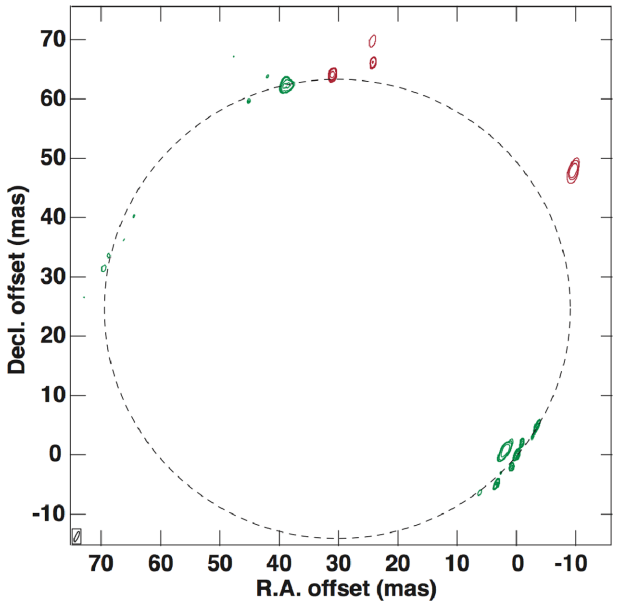

Fig. 3. Composite map of SiO masers of $v = 2$ (green) and $v = 3$ (red) ($J = 1 \rightarrow 0$) around W Hya observed on 2012 May 21 ($\phi = 0.03$). The dashed circle is drawn so as to fit to the $v = 2$ maser distribution with a diameter of 77 mas. The brightest $v = 2$ and $v = 3$ maser spots are located at (0 mas, 0 mas) and (32 mas, 62 mas), respectively. The contour levels are set at 1.8, 8.8, 18, 44, 88, 128, and 158 Jy km s^{-1} beam^{-1} for the $v = 2$ masers and 0.04, 0.27, 0.53, 1.3, 2.6, 3.7, and 4.6 Jy km s^{-1} beam^{-1} for the $v = 3$ masers.

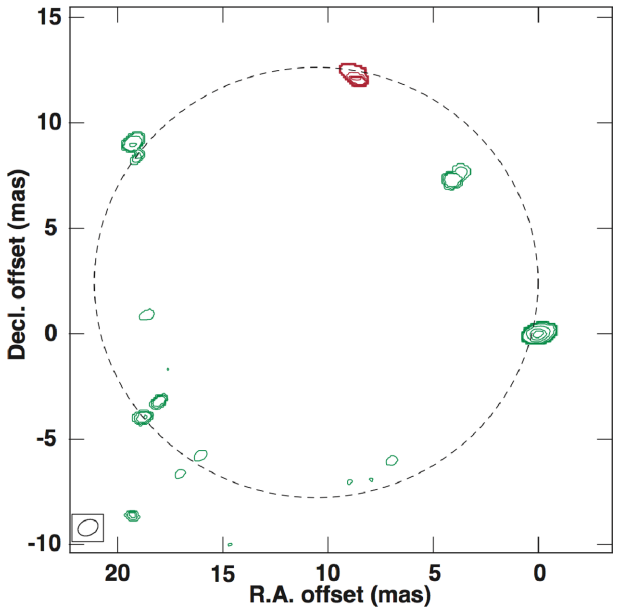

Fig. 4. Same as figure 3, but around WX Psc. The dashed circle is drawn so as to fit to the $v = 2$ maser distribution with a diameter of 21 mas. The contour levels are set at 0.4, 1.9, 3.7, 9.5, 19, 26, and 34 Jy km s^{-1} beam^{-1} for the $v = 2$ masers and 0.02, 0.11, 0.24, 0.57, 1.2, 1.6, and 2.1 Jy km s^{-1} beam^{-1} for the $v = 3$ masers.

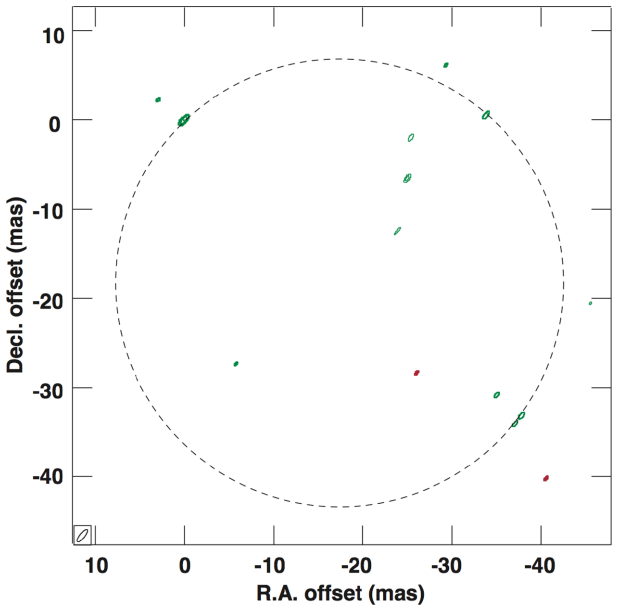

Fig. 5. Same as figure 3, but around R Leo observed on 2012 May 21 ($\phi = 0.18$). The dashed circle is drawn so as to fit to the $v = 2$ maser distribution with a diameter of 50 mas. The brightest $v = 2$ and $v = 3$ maser spots are located at (0 mas, 0 .mas) and (−26 mas, −32 mas), respectively. The contour levels are set at 0.03, 1.6, 3.3, 16, 23, 28, and 32 Jy km s^{-1} beam^{-1} for the $v = 2$ masers and 0.08, 4.1, 8.3, 21, 41, 58, 70, and 75 mJy km s^{-1} beam^{-1} for the $v = 3$ masers.

were fitted with a circle roughly by eye on the assumption that gas is uniformly released from the central star to form a spherical envelope and the masers are tangentially beamed in the CSE shell. This assumption is more or less supported by previous VLBI observations (e.g., Imai et al. 2010; Gonidakis et al. 2013). Thus the distances of individual maser spots from the central star can be measured as radial distances from the center of the ring.

In T Cep, the $v = 3$ maser features are aligned in the south-east side of the ring and coincident with the $v = 2$ masers within ∼2 mas (∼0.3 au). Figure 2b shows the first moment maps for T Cep. There exist two maser feature groups with radial velocities (with respect to the local standard of rest) of −4 km s^{-1} and −6 km s^{-1} for both of the two lines. The two lines coexist in each of the groups within ∼1 km s^{-1}. This supports that the spots of the $v = 2$ and $v = 3$ masers coexist in physically common regions.

In W Hya, the location of the brightest feature of the $v = 3$ maser has an offset of ∼7 mas (0.6 au) from the closest feature of the $v = 2$ maser. Some of the $v = 3$ masers are located outside of ∼7 mas (0.6 au) from the $v = 2$ maser ring. This looks to be the same trend as that reported by Oyama et al. (2016), in which the masers in W Hya were observed on 2016 May 8 ($\phi = 0.69$) and May 27 ($\phi = 0.74$). In the case of WX Psc, only one $v = 3$ maser spot was detected with an offset of ∼7 mas (9 au) from the closest $v = 2$ maser spot, although the $v = 3$ spot was on the $v = 2$ ring. For the case of R Leo, the $v = 3$ masers exist in regions ∼7 mas (0.7 au) away from the $v = 2$ region.

4 Discussion

According to a theoretical model (Desmurs el al. 2014), the H_2O–SiO line-overlapping mechanism is expected to actually work on the maser excitation in the case where one can see overlapping of the $v = 3$ maser regions with the $v = 2$ maser regions, as seen toward T Cep. Although the model does not deal with the excitation of the $v = 3$ maser in detail, we expect that it can also be explained in the same manner as the excitation of the $v = 1$ and $v = 2$ masers. The sequence of line-overlapping processes may be as follows: (1) the stellar light curve reaches its maximum; (2) the ∼8.2 μm emissions from H_2O molecules become strong as the MIR radiation from the star increases, perhaps together with the external dust region being heated by the stellar light; (3) SiO molecules are excited from $v = 1$ $J = 0$ to $v = 2$ $J = 1$ and from $v = 2$ $J = 0$ to $v = 3$ $J = 1$ by the H_2O transitions of $11_{6,6}$ $v_2 = 1 \rightarrow 12_{7,5}$ $v_2 = 0$ (8.2025 μm) and $5_{0,5}$ $v_2 = 2 \rightarrow 6_{3,4}$ $v_2 = 1$ (8.23312 μm), respectively; (4) the $v = 3$ $J = 1 \rightarrow 0$ maser grows around the $v = 2$ $J = 1 \rightarrow 0$ maser region.

On the other hand, line-overlapping is expected to be inefficient for stars that do not show the spatial correlation as seen in W Hya, WX Psc, and R Leo. In such cases, the $v = 3$ masers are likely excited only by collisional excitation as a dominant mechanism, which may be caused by shocks around the pulsating star (e.g., Gonidakis et al. 2013). Note that, in W Hya and R Leo, the $v = 3$ maser spots often exist at larger distances from the central stars than the $v = 2$ maser regions. Since the energy level of the $v = 3$ vibrational excitation state of an SiO molecule is higher than that of the $v = 2$ level, this larger distance of $v = 3$ maser spots indicates that the gas extends asymmetrically to propagate shocks to such distant regions from the star.

The efficiency of the line-overlapping should have a correlation with the MIR emission from H_2O molecules. Taking into account the phase lags of $\phi \sim 0.1$–0.2 between the maximum of the infrared and optical light curve in Mira variables (Smith et al. 2006), the line-overlapping would work most efficiently at $\phi \sim 0.1$–0.2 of the optical light curve. T Cep, R Leo, and W Hya were observed at $\phi = 0.28$, $\phi = 0.18$, and $\phi = 0.03$, respectively. The two line observations have been made for W Hya at $\phi = 0.11$ and $\phi = 0.22$ by Imai et al. (2010) and $\phi = 0.69$ and $\phi = 0.74$ by Oyama et al. (2016), and the overlap between the two lines was seen only at $\phi = 0.22$. For further statistical discussion, we revisited the composite maps of the $v = 1$, $v = 2$, and $v = 3$ masers reported by Desmurs el al. (2014). They observed R Leo, TX Cam, U Her, and IK Tau at $\phi = 0.17$, $\phi = 0.02$,

Table 2. Stellar light-curve phase.

Source name	Phase*	Phase at the minimum†	Line-overlapping‡	Observation date§	Period‖ [d]
W Hya	0.11	0.50		2009 Feb 27–28(I)	390
	0.22		Y	2009 Apr 11–12(I)	
	0.03			2012 May 21	
	0.69			2013 May 8(O)	
	0.74			2013 May 27(O)	
R Leo	0.17	0.57		2009 Nov 13(D)	310
	0.18			2012 May 21	
T Cep	0.28	0.46	Y	2012 May 22	388
TX Cam	0.02	0.47	Y	2010 Jan 31(D)	557
U Her	0.29	0.56	Y	2011 Apr 17(D)	404
IK Tau	0.13	0.50	Y	2011 Nov 4(D)	470

*Same as table 1.
†The light curve becomes the minimum at this phase estimated using the data from AAVSO. The symmetrical light curve becomes the minimum at the phase of 0.50.
‡Y: The $v = 3$ masers overlap with the $v = 2$ masers.
§We investigate the correlation of maser distributions with the light curve using the composite maps obtained by the previous studies: (I) Imai et al. (2010); (O) Oyama et al. (2016); (D) Desmurs et al. (2014).
‖Period of stellar light curve from AAVSO.

$\phi = 0.29$, and $\phi = 0.13$, respectively, and fitted a ring-like brightness distribution to each of the observed maser lines using the regression package ODRpack. Although the ring sizes are not completely equal, these masers are well coincident when taking into account the widths of the rings. In TX Cam, U Her, and IK Tau, the $v = 3$ masers correlate with the $v = 2$ masers in position within the typical size of SiO maser spots of ∼5 mas corresponding to ∼2 au, ∼1.8 au, and ∼1.5 au, respectively, suggesting that the line-overlapping mechanism worked in the three stars. In R Leo, it is difficult for us to judge the reliability of the superposition of the $v = 3$ maser map, because of the failure to fit any circle for the $v = 3$ masers due to a poor number of spots.

Table 2 summarizes the light curve phases, and our judgment of the maser distributions of the six stars. The $v = 3$ masers coexist with the $v = 2$ masers at the phase of $\phi = 0.0$–0.3 in five out of the six LPVs. Focusing on W Hya, the line-overlapping worked only at $\phi = 0.22$ and did not work at the other four phases. Thus, the line-overlapping mechanism seems to become efficient soon after the light curve maximum and is then inefficient as the light curve approaches the minimum, while the collisional pumping works during the whole light curve cycle, as mentioned in section 1. In fact, in W Hya, the phase ($\phi = 0.22$) when the line-overlapping works is almost coincident with the duration of MIR light curve maximum ($\phi = 0.15 \pm 0.05$; Zhao-Geisler et al. 2011).

On the other hand, overlap between the $v = 2$ and $v = 3$ masers in R Leo was not observed even at $\phi = 0.17$. This might be due to a poor probability of high gains and observable beaming of the maser emission and/or intrinsic characteristics of the star that affect maser excitation such as the luminosity and/or chemical composition of the star. In order to investigate the excitation of the $v = 3$ masers and the light curve, we have carried out multi-epoch observations towards R Leo and IK Tau in 2017 using VERA, NRO, and the Kashima 34 m telescope. The results will be published separately.

Note that cancelation of the population inversion between the $v = 2$ $J = 2$ and the $J = 1$ levels occurs during the whole light curve cycle according to the previous statistical studies by Olofsson, Rydbeck, and Nyman (1985) and Bujarrabal et al (1996), which suggest the anomalous weakness of the $v = 2$ $J = 2 \rightarrow 1$ masers in oxygen-rich stars. This supports the hypothesis that line-overlapping in the $v = 1$ $J = 0$ to $v = 2$ $J = 1$ transition works during the whole light curve cycle. The case of the $v = 3$ masers was investigated by Cho, Lee, and Park (2007), who carried out single-dish observations of the $v = 3$ $J = 2 \rightarrow 1$ and $J = 3 \rightarrow 2$ towards oxygen-rich stars TX Cam ($\phi = 0.96$), R Aqr ($\phi = 0.82$), R Cas ($\phi = 0.05$, 0.73, 0.80, and 0.86), W Hya ($\phi = 0.47$, 0.60, and 0.67), and R Leo ($\phi = 0.61$, 0.66, 0.73, and 0.76). They found that the $v = 3$ $J = 2 \rightarrow 1$ maser line was not detected towards all oxygen-rich stars, while the $v = 3$ $J = 3 \rightarrow 2$ maser line was detected towards only TX Cam around $\phi = 0.00$ in the sources surveyed. We cannot rule out the possibility that the quenching of the population inversion between the $v = 3$ $J = 2$ and $J = 1$ levels has not occurred towards those stars except TX Cam because the $v = 3$ masers are often too faint to be detected beyond the light maximum. It is difficult to discuss such correlation in the present paper. Neither can we rule out the possibility that the line-overlapping in the

$v = 2$ $J = 0$ to $v = 3$ $J = 1$ transition will be canceled beyond the duration from the light maximum to the minimum. We need to conduct multiple-epoch VLBI observations including the $v = 3$ $J = 1 \rightarrow 0$ line for a few cycles to clarify the duration when the line-overlapping could be dominant.

Acknowledgments

The VERA/Mizusawa VLBI observatory and Nobeyama Radio Observatory are branches of the National Astronomical Observatory of Japan, an inter-university research institute operated by the Ministry of Education, Culture, Sports, Science and Technology. M. O. and H. I. are supported by the KAKENHI program (16H02167) of the Japanese Society for Promotion of Science (JSPS) and Commissioning Research Project funded by the Korea Astronomy and Space Science Institute, which is under the protection of the National Research Council of Science and Technology. J. N. was supported by the Ministry of Education and Science of the Russian Federation Agreement no. 02.A03.21.0006. We acknowledge with thanks the variable star observations from the AAVSO International Database contributed by observers worldwide and used in this research.

References

Bujarrabal, V. 1994, A&A, 285, 953
Bujarrabal, V., Alcolea, J., Sánchez Contreras, C., & Colomer, F. 1996, A&A, 314, 883
Chibueze, J. O., Miyahara, T., Omodaka, T., Ohta, T., Fujii, T., Tanaka, M., Motohara, K., & Miyoshi, M. 2016, AJ, 817, 115
Cho, S.-H., Kaifu, N., & Ukita, N. 1996, AJ, 111, 1987
Cho, S.-H., Lee, C. W., & Park, Y. -S. 2017, ApJ, 657, 482
Choi, Y. K., Hirota, T., Honma, M., & Kobayashi, H. 2008, in IAU Symp. 248, A Giant Step: from Milli- to Micro-arcsecond Astrometry, ed. W. J. Jin et al. (Cambridge: Cambridge University Press), 192C
Desmurs, J. -F., Bujarrabal, V., Lindqvist, M., Alcolea, J., Soria-Ruiz, R., & Bergman, P. 2014, A&A, 565, A127
Gonidakis, I., Diamond, P.J., & Kemball, A. J. 2013, MNRAS, 433, 3133
Gordon, I. E., et al. 2017, J. Quant. Spectrosc. Radiat. Transfer, 203, 3
Gray, M. 2012, Maser Source in Astrophysics (Cambridge: Cambridge University Press), 162
Imai, H., et al. 2012, PASJ, 64, L6
Imai, H., Nakashima., J.-I., Deguchi, S., Yamauchi, A., Nakagawa, A., & Nagayama, T. 2010, PASJ, 62, 431
Lockett, P., & Elitzur, M. 1992, ApJ, 399, 704
Olofsson, H., Rydbeck, O. E. H., Lane, A. P., & Predmore, C. R. 1981, ApJ, 247, L81
Olofsson, H., Rydbeck, O. E. H., & Nyman, L.-Å. 1985, A&A, 150, 169
Oyama, T., et al. 2016, PASJ, 68, 105
Smith, B. J., Price, S. D., & Moffett, A J., 2006, AJ, 131, 612
Soria-Ruiz, R., Alcolea, J., Colomer, F., Bujarrabal, V., Desmurs, J.-F., Marvel, K. B., & Diamond, P. J. 2004, A&A, 426, 131
Tipping, R. H., & Chackerian, C., Jr. 1981, J. Mol. Spectrosc., 88, 352
van Leeuwen, F. 2007, A&A, 474, 653
Whitelock, P. A., Fest, M. W., & van Leeuwen, F. 2008, MNRAS, 386, 313
Yun, Y. J., et al. 2016, ApJ, 822, 3
Zhao-Geisler, R., Quirrenbach, A., Köhler, R., Lopez, B., & Leinert, C. 2011, A&A, 530, A120